Protocol-Level Understanding of the Aggregate Interference in Random CSMA/CA Networks

June Hwang†, Riku Jantti, and Seong-Lyun Kim,

***Abstract*— In this paper, we investigate the cumulative distribution function (CDF) of the aggregate interference in carrier sensing multiple access/collision avoidance (CSMA/CA) networks measured at an arbitrary time and position. We assume that nodes are deployed in an infinite two-dimensional plane by Poisson point process (PPP) and the channel model follows the singular path loss function and Rayleigh fading. To find the effective active node density we analyze the distributed coordinate function (DCF) dynamics in a common sensing area and obtain the steady-state power distribution within a spatial disk of radius $R/2$, where R is the effective carrier sensing distance. The results of massive simulation using Network Simulator-2 (NS-2) show a high correlation with the derived CDF.**

***Index Terms*— Aggregate interference, CSMA/CA, DCF, Poisson point process, NS-2**

I. Introduction

A. Motivations

Due to the inherent scarcity of frequency spectrum and increasing wireless traffic demands nowadays, frequency reuse has become an essential key technological issue associated with contemporary wireless communication systems. Frequency reuse intrinsically causes interference between wireless links in not only homogeneous but also heterogeneous systems using the same frequency. Accordingly, the state of the aggregate interference at an arbitrary position in the random node topology has become of great importance.

In this paper, we are interested in the aggregate interference of carrier sense multiple access/collision avoidance (CSMA/CA) networks. Our motivation is two-folds: The first motivation is associated with the prevalence of this random access network. WiFi that complies with IEEE 802.11 standards offloads the traffic from conventional wireless cellular systems. In reality, this support from WiFi systems helps current cellular systems to manage the ever-increasing traffic without urgent and huge amounts of investments in system upgrades, and this is likely to last for a while. Additional merits of the WiFi system include the fact that it is cheap and easy to set up without any spectrum-licensing procedures. As a result of these benefits, WiFi access points (APs) and compliant stations such as laptops, smartphones, and even smart TVs are being deployed more frequently by end users and office administrators, as well as wireless service providers in homes, offices, automobiles, and public areas. Even more of these devices will be deployed when advanced amendment standards such as IEEE 802.11 ac, ad, af, and ai are finalized and implemented.

Our second motivation is the fact that it is more difficult to control interference in this random access network than in centralized systems even though the interference is crucial in both systems. Unlike the former system, which is designed for proactively controlling the interference between the communicating entities and managing the spectrum resources in the central control unit, the latter system has no global control unit. A mechanism called intercell interference coordination (ICIC) [1], [2] has already been proposed to resolve the mutual interference in the former system and it is highly likely that it will be implemented in practice, although some amount of modification may be necessary. In contrast, WiFi was designed without considering interference among overlapped basic service sets (OBSSs). In addition, coordination between multiple WiFi cells calls for policy-level negotiation among different WiFi service operators, which is an untenable issue in the technology domain. Therefore, controlling mutual interference in random access networks is more problematic than in controlled counter systems.

For these reasons, we believe that studying the characteristics of the aggregate interference with a view toward using this knowledge to craft realistic solutions can solve the uncontrollable interference problem in the WiFi arena. Within this context, we investigate the aggregate interference in randomly deployed IEEE 802.11 distributed coordination function (DCF) networks (we prefer this standard name instead of simply WiFi so as to explicitly incorporate the PHY and MAC layer operations) in this paper. From an understanding of the distribution of the aggregate interference at the protocol level, we can control this interference using the relationships discovered among the protocol parameters. Since to date there has been no test at the simulator level for aggregate interference, we test as well as analyze the interference at the protocol level. It is difficult to apply the measurements from the test bed to statistical inference on interference power distribution because signals are vulnerable to many unknown factors in the testing circumstance and massive variations in node geometry are hard to be set up in the real test bed. Simulator-level tests can however overcome all of these weaknesses associated with real measurements. There is no unknown factors to affect aggregate power in the simulator and numerous changes in node geometry are possible. Consequently, our goal in this study is to obtain the statistical inference of the aggregate interference and verify the results via simulation.

J. Hwang is with School of Integrated Technology, Yonsei University, Incheon, Korea. Email: june.hwang@yonsei.ac.kr. R. Jantti is with Department of Communications and Networking, School of Electrical Engineering, Aalto University, P.O. Box 13000, FI-00076 Aalto, Finland. Email: riku.jantti@aalto.fi. S.-L. Kim is with Department of Electrical and Electronic Engineering, Yonsei University, Seoul, Korea. Email: slkim@yonsei.ac.kr. † The corresponding author is J. Hwang.

Most of the work previously done in this area focused on ALOHA-like systems in which the aggregate interference can be analyzed by assuming that transmitting nodes have independent locations and behaviors [3], [4]. Although broadband cellular systems such as LTE, LTE-A, WCDMA or its femto cell networks can also be modeled using this transmission-independent behavior, this is not a realistic assumption for CSMA/CA networks in which a certain interference level always needs to be maintained in a distributed manner. In a network of CSMA/CA nodes, every communication entity first senses the ongoing transmission in the channel and then determines when to start transmitting. The inappropriateness of the independent model in such a scenario was noted in [5], in which the authors proposed the alternative dependent point process to mimic real CSMA/CA networks. However, this proposed point process still cannot describe the DCF operation, in which collision and idle time, as well as successful transmission, can occur even in the exclusion area by carrier sense. Compared with these previous research efforts, to the best of our knowledge, our work is the first to investigate the exact distribution of aggregate interference in CSMA/CA networks and to validate it by means of massive simulations.

B. Summary of contributions and organization of this paper

Our paper has the following notable results:

- **Owing to the possibility of concurrent transmission incurred by DCF operation occurring within an exclusion area, CSMA/CA random networks can only be modeled by the Poisson point process (PPP), not the dependent point process.** Section II addresses the difference between the dependent and independent point processes, and explains how real CSMA/CA networks can be dealt with.
- **We derive the effective node density reflecting CSMA/CA MAC layer operation.** Section III explains this. This section is the core of our work since all the cross-layer parameters are coupled to model the network behavior. Further, this is used in PPP shot noise analysis, which is the result of the first item.
- **Aggregate interference in PPP shot noise analysis using our derived effective node density is verified using the NS-2 network simulator and Matlab simulations.** Unlike other related theoretical analyses of stochastic geometry researches, we verify exactly how much our model reflects the NS-2 simulation results. We also compare our results with the Matlab simulation on dependent point processes and thereby show that the PPP model with our new effective node density performs the best in modeling the aggregate interference. Related issues are outlined in Section IV.

Concluding remarks are given in Section V. A compact form of shot noise analysis [6] follows in the Appendix.

II. Point process for modeling random CSMA/CA networks

In this section, we focus on determining which type of point process is suitable for modeling CSMA/CA networks. A generic wireless network consisting of multiple randomly deployed nodes can be described via a point process. In the point process, a mark (a scalar or a vector) can be assigned to each point independently, which is useful for modeling node-oriented properties such as transmission power, medium access delay. In particular, the case where the number of nodes in a network is Poisson-distributed and their positions at a given time instant are independent of each other, is adequately explained by means of the PPP. The method to derive the aggregate power emitted from points at an arbitrary position under independent marked PPP was previously studied as *shot noise field*, which was originally used to model the noise in electronic circuits in the time domain [7].

A. Inappropriateness of PPP for CSMA/CA modeling

However, the PPP approach as it currently exists is insufficient to model the CSMA/CA. The reason is that the carrier sensing philosophy is not reflected in it. PPP is a typical *independent* point process in which the points are deployed independently of each other. On the other hand, in the carrier sensing (CS) operation, a sensing node always senses the shared medium and it delays its transmission once it senses that the medium is busy. The result is that active nodes are affected by each other, which means that the process is not independent.

B. Inappropriateness of the dependent point process

Let us now consider the dependent point process as a possible alternative. Here, the dependent point process means that some initially deployed points are discarded or selected by the metric related to the other points' marks or locations. To the best of our knowledge, there are two dependent point processes most related to the modeling of CSMA/CA networks: the Matern hardcore (MHC) process and the simple sequential inhibition (SSI)- point process. In [5], the authors are also motivated by the inappropriateness of PPP, i.e., the independence of points. In the paper, they compared the aggregate power distributions of PPP, MHC, and SSI with simulations, and concluded that SSI is the most appropriate one for modeling CSMA networks. However, their result is not fully acceptable because the operation they used in the simulation was not the real one but a modified version of a dependent point process based on IEEE 802.15.4 PHY parameters. More specifically, they neither considered any details of practical MAC layer parameters nor channel characteristics. Leaving this result aside, their MHC and SSI are fundamentally based on the hard exclusion area; nevertheless, they contain ambiguities in the determination of this area. To further illustrate the issue, let us look at our simulation results.

We simulated a realistic CSMA/CA random network using NS-2 in order to observe the concurrent transmission behavior. Fig. 1 shows our simulation topology and the effect on the distribution of the number of concurrent transmitting nodes. In the grid topology, the black dot represents the transmitter and the corresponding receiver is located at 5 (m) right and 5 (m) up away from its transmitter; the receiver is omitted from the figure. In the simulation, a 500 B payload was given to each

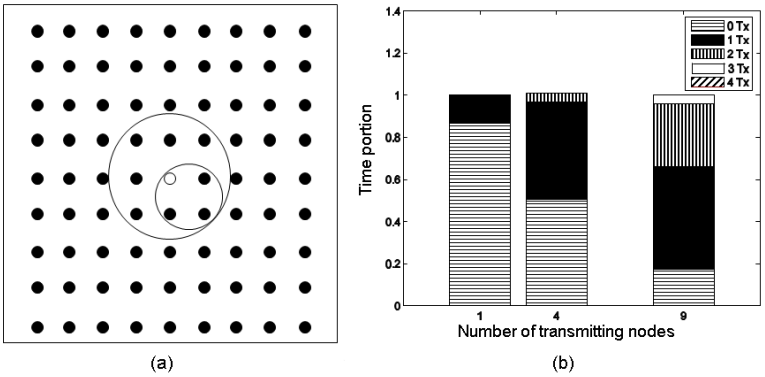

Fig. 1. The number of transmitting nodes concurrently: (a) scenario and (b) result.

transmitter and the traffic was saturated. The distance between the two nearest black dots was 50 (m), and the CS threshold was tuned so that the resulting CS range was 70 (m), derived using Equation (4). All other parameters were the same as those in Table III. The large circle in the center denotes a CS area based on the white dot (one of the transmitters), while the smaller circle has a radius that is one half of the CS range. The relative time durations for each set of concurrent transmissions are depicted in the bar plot.

In the graph, two things are of note: First, there is a time period in which two nodes are concurrently transmitting when all transmitters are even in each other's CS area (see the 4 nodes case in the bar plot). Second, there is a time period in which the medium is idle in the full CS area (node 9 case). The first case occurs due to CS failure or collision in real situation. MHC and SSI are fully *dependent thinning* of PPP with the exclusion area, and they cannot model these events. The resulting effective node density of the dependent point process is likely to be lower than that of the real one. These approaches may work well in collision-less CSMA/CA networks where slot time is zero and backoff time is a continuous random variable (RV) [8], rather than real situations. The second case occurs due to the idle time from the binary exponential backoff (BEB) and the DCF. This waste of time resource is the intrinsic cost of the distributed random access MAC. In the dependent point process, any point having none of the other points in its exclusion area always survives. The resulting effective node density of this process is likely to be higher than that of the real one. *As a result, the real operation of a CSMA/CA network has both factors having higher and lower effective node density than that of the dependent point process.* This difference is from the lack of MAC layer operation modeling in the dependent point process.

C. Review of PPP

As will be shown in Section III-B.1, these collision events occur with a certain probability in real situations. This means that the concurrent transmission in an exclusion area occurs with some probability, not with deterministic patterns. This stochastic characteristic of real networks is appropriately modeled using the independent point process. Therefore, we believe that a possible way to model a CSMA/CA network is again to use PPP, but with a *new* effective active node density reflecting MAC layer operation.

This is notable since recent research efforts such as [4] and literatures therein point out that CSMA/CA can be modeled with MHC point process, which is different from our conclusion. At the very least, the aggregate power at an arbitrary position can be elaborated more when using PPP with a new effective node density rather than pure PPP or MHC/SSI.

III. Effective Active Node Density

In the infinite plane, the nodes in a CSMCA/CA network are coupled with each other via the shared medium. The number of neighbor nodes, relative distances among nodes, and the current state/history of MAC and PHY/MAC/NET layer parameters of nodes in the local shared medium are again the factors affecting the states of their media. Moreover, this medium itself does not have a deterministic boundary but a random one since the channel link gain is varies continuously. Therefore, obtaining information on when and who is "on" is not straightforward even in a closed spatial domain.

To resolve this difficulty, we first convert this local medium of a transmitting (or sensing) node from stochastic to deterministic using the equal sensing resolution concept in Section III-A. The medium here is thought of as a kind of two-dimensional space. The infinite plane is then regarded as the union, where this local medium of the same size is filled. Once the spatial boundary of this local medium is given as deterministic, N, the number of deployed nodes in this boundary is obtained using PPP. N_a, the number of active nodes in this boundary should be found based on this N, and the transmission power distribution in this boundary can be found based on N and N_a.

These parameters are all analyzed based on the local shared medium called *basic independent unit* in this paper. By the homogeneity of PPP (**Definition 2.** in Appendix), the number of deployed nodes in the same area has the same probability mass function (PMF) regardless of its shape and location. Therefore, wherever the basic independent unit is, the number of nodes therein has identical PMF. Every related analysis is a function of this number of nodes.

A. Carrier Sensing

We introduce an effective CS range R so that a sensing node can sense any on-going transmission in this range and cannot sense any transmission outside of this area. By making the stochastic CS boolean, the complexity of the problem can be reduced. Then within the disk of radius $\frac{R}{2}$, every node senses each other. We set this disk as a basic independent unit.

CS is based on the threshold γ, i.e., if the sensed power level at a sensing node is greater or lower than γ, a sensing node regards the channel is busy or idle, respectively. Assuming there is only one interferer near the sensing node (i.e., we count only the nearest one if there are multiple interferers), the CS probability versus the distance to this interferer is calculated as followings:

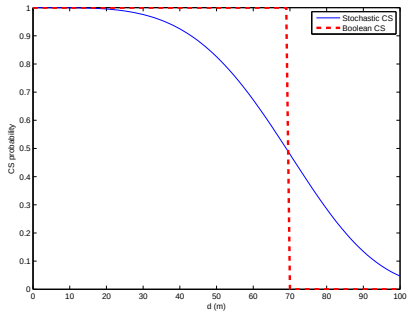

Fig. 2. $\Pr[\frac{p_i}{d^4} + \nu \geq \gamma]$ for varying distance d. $p_i \sim \text{Exp}(1/p)$. γ is given as $p/75^4$ where $p = 0.001(W)$ and noise $\nu = 10^{-12}(W)$. In this example, R is calculated to be 70(m).

$$\mathbb{P}[\text{Channel is busy}] = \mathbb{P}[\frac{p_i}{r^4} + \nu \geq \gamma], \tag{1}$$

where p_i is a RV representing the product of the fading effect and the constant transmission power from a typical node i, r is the distance between the sensing node and interferer, and ν is the receiver noise power. Considering Rayleigh fading in (29), p_i follows $\text{Exp}(1/p)$ with a constant transmission power p.

Consequently, by the aforementioned definition of R, we convert the stochastic CS to a deterministic one. First, the average sensing area is calculated by integrating the parts of the circumference, of which the radius and the center are r and the sensing node, respectively. The CS probability of a point on this circumference is from (1).

$$\begin{aligned} & \int_0^\infty 2\pi r \cdot \mathbb{P}[\frac{p_i}{r^4} + \nu \geq \gamma] \mathrm{d}r \\ = & \int_0^\infty 2\pi r e^{-\frac{1}{p}(\gamma-\nu)r^4} \mathrm{d}r \\ = & \frac{\pi^{3/2}}{2\sqrt{\frac{\gamma-N}{p}}} \end{aligned} \tag{2}$$

Using the fact that the deterministic CS region should have the same average sensing area (sensing resolution) as the stochastic CS, the following equation is derived:

$$\frac{\pi^{3/2}}{2\sqrt{\frac{\gamma-N}{p}}} = \pi R^2 \tag{3}$$

Finally, we get the CS distance R as follows:

$$R = \frac{1}{\sqrt{2}} \left(\frac{\pi p}{\gamma - N} \right)^{1/4} \tag{4}$$

By this deterministic CS distance, the interference is regarded as boolean at a given distance rather than stochastic.

Let us consider an infinite plane with the nodes randomly deployed. Delineating an arbitrary disk having of radius $R/2$ in the plane, we denote this area by the *sharing area*,[1] where every nodes in this area can sense other nodes' transmissions by the definition of CS range R. By PPP, the number of deployed nodes in a sharing area follows Poisson distribution with the parameter $\lambda\pi(\frac{R}{2})^2$ as follows:

$$\mathbb{P}[N = n] = \frac{\{\lambda\pi(\frac{R}{2})^2\}^n}{n!} \exp(-\lambda\pi(\frac{R}{2})^2) \tag{5}$$

Once we know N, we subsequently derive the number of active nodes and the power distribution at an arbitrary time instant in the sharing area. These will be explained in the following sections.

B. Steady-state power distribution in a sharing area

Definition 1. p_{on} is the probability that there are on-going transmissions in a given sharing area at a certain time.

So far we have derived $\mathbb{P}[N = n]$ and we will derive $\mathbb{P}[N_a = a|N = n]$ based on p_{on}.

1) DCF dynamics in a sharing area: Consider the IEEE 802.11 DCF protocol for CSMA/CA MAC. If all the transmitting nodes can sense each other in a sharing area and the given traffic to each node is a saturated one, we know the steady-state behavior in this area. As shown in [9] and subsequent research efforts, the backoff stage of each node in the network is random at a certain time and this can be elaborated through a two-dimensional Markov chain. We have two main quantities for addressing this: p_c is the probability that the collision happens conditioned on the transmission of each node, and τ is the transmission probability of a node at a randomly chosen time slot. These two quantities are derived by finding the steady-state solution of the discrete time Markov chain.

By following the notations of [10], we have the BEB dynamics with m maximum backoff stage, K maximum retry limit and W_0 initial window size. The backoff period durations $U^{(i)}, i = 0, \ldots, K-1$, are discrete uniform random variables given by:

$$U^{(i)} = \begin{cases} \mathcal{U}(0, 2^i W_0 - 1), & i = 0, \ldots, m, \\ \mathcal{U}(0, 2^m W_0 - 1), & i = m+1, \ldots, K-1 \end{cases} \tag{6}$$

where $\mathcal{U}(a, b)$ is the uniform distribution with the outcome interval $[a, b]$. From this, the average backoff durations are:

$$E[U^{(i)}] = \begin{cases} (2^i W_0 - 1)/2 & \text{for } i = 0, \ldots, m \\ (2^m W_0 - 1)/2 & \text{for } i = m+1, \ldots, K-1 \end{cases} \tag{7}$$

For a bigger size of data packet than an *RTSthreshold* in standard [11], K follows Long Retry Limit (the practical value is 4). Otherwise it follows Short Retry Limit (the practical value is 7)[2]. Let π_i denote the relative frequency that a node enters the ith retransmission phase in the steady state. Then, it is shown that:

$$\pi_i = (1 - p_c) p_c^i (1 - p_c^K)^{-1}, \tag{8}$$

[1]This has the same object as the basic independent unit, i.e., the spatial unit where we can model the activity of nodes therein. However we use this term when explaining CS operation.

[2]Refer to the simulation parameters in Table III.

and the probability τ that a node transmits in a randomly chosen time slot is:

$$\tau = \left\{ \sum_{i=0}^{K-1} \pi_i E[U^{(i)}] \right\}^{-1} = \left\{ \frac{(1-p_c)W_0(1-(2p_c)^m)}{2(1-p_c^K)(1-2p_c)} + \frac{2^m W_0(p_c^m - p_c^K)}{2(1-p_c^K)} - \frac{1}{2} \right\}^{-1}. \quad (9)$$

Again, p_c is obtained through:

$$p_c = 1 - (1-\tau)^{N_a - 1}, \quad (10)$$

where N_a is the number of active (contending) users. The probability that a transmitted packet encounters a collision, is the probability that, in a time slot, at least one of the remaining stations transmit.

We can solve the system dynamics by solving two independent Equations (9) and (10) and the existence of this solution is guaranteed by the fixed point theorem [9].

2) Power distribution in a sharing area: Since we know τ, we can obtain the steady state power density. The probability that i nodes transmit simultaneously at an arbitrary time slot, given that N_a transmitting nodes are deployed in a sharing area is:

$$p_a(m) = \mathbb{P}[i = m | N_a = a] = \binom{a}{m} \tau^m (1-\tau)^{a-m} \quad m = 0, \ldots, a. \quad (11)$$

Each transmitting node's operation in a sharing area is synchronized since the medium is sensed perfectly and every node has the inner clock. Thus, idle time is also segmented into multiple slot times (σ). Therefore, all events (idle time slot, successful and collision time slot) can be distinguished by their durations. At an arbitrary time, the sharing area medium is in one of three events and we call this random time slot as the *virtual time slot*. The virtual time slot has the random duration T_v. We assume that the payload size is the same as PAY for all nodes. In basic mode,

$$T_v = \begin{cases} \sigma, \\ \text{ for the idle slot time,} \\ T_s^{BAS} (= PHY + \lceil \frac{(MAC+PAY)}{R_s} \rceil T_s + sifs + ACK \\ + difs), \text{ for the successful slot time,} \\ T_c^{BAS} (= PHY + \lceil \frac{(MAC+PAY)}{R_s} \rceil T_s + difs), \\ \text{ for the collision slot time,} \end{cases}$$

where PHY, $sifs$, ACK, $difs$ are the durations for PHY header, SIFS time, ACK packet, DIFS time respectively. And MAC, R_s and T_s are the MAC header size, symbol rate and symbol duration respectively. Once the transmission starts, irrespective of success or not, the packet of size $PHY + \lceil \frac{(MAC+PAY)}{R_s} \rceil T_s$ is transmitted first. And then the remaining parts ($sifs + ACK + difs$ or $difs$) are determined according to the existence of collision. Of course, in RTS-CTS mode, successful slot time and collision slot time will be changed into $T_s^{RTS} (= RTS + CTS + PHY + \lceil \frac{(MAC+PAY)}{R_s} \rceil T_s + 3 * sifs + ACK + difs)$ and $T_c^{RTS} (= RTS + difs)$ respectively. RTS and CTS are the duration of RTS and CTS packet, respectively.

T_v has the PMF induced from (11) such as $p_a(0)$, $p_a(1)$, and $1 - p_a(0) - p_a(1)$ are for idle, successful transmission, and collision events, respectively. We derive the mean virtual time slot, $\mathbb{E}[T_v]$ using this PMF in each mode.

$$\mathbb{E}[T_v^{BAS}] = \sigma p_a(0) + T_s^{BAS} p_a(1) + T_c^{BAS}(1 - p_a(0) - p_a(1)),$$
$$\mathbb{E}[T_v^{RTS}] = \sigma p_a(0) + T_s^{RTS} p_a(1) + T_c^{RTS}(1 - p_a(0) - p_a(1)).$$

The distribution of the number of concurrent transmissions (which is also the power distribution) is based on this PMF. In each virtual slot, the number of concurrent transmissions is various from 0 to N_a. And even when the number of concurrent transmitting nodes are given, the virtual slot consists of nobody transmission portion and somebody transmission portion. In the basic mode, nobody transmits during σ. During $sifs$ and $difs$ in the both of successful and collision slot time, nobody transmits, too. During packet transmission time ($PHY + \lceil \frac{(MAC+PAY)}{R_s} \rceil T_s$ and ACK) in a successful slot, one node transmits, while multiple nodes transmit during $PHY + \lceil \frac{(MAC+PAY)}{R_s} \rceil T_s$ in a collision slot. In RTS-CTS mode, the power density is changed in the same manner. Therefore, the actual power distribution, $\mathbb{P}[j \text{ nodes transmit} | N_a = a]$ is obtained using this distribution in the basic mode (Equation (12)) and RTS mode (Equation (13)). The probability of busy channel in a sharing area p_{on} is $\sum_{j=1}^{a} B_a^{BAS/RTS}(j) = 1 - B_a^{BAS/RTS}(0)$.

C. Number of active nodes in a sharing area

Consider a given sharing area H. Let *sensing area* be defined as the sensing node's CS area excluding H. (See the asymmetric donut in Fig. 3 for the relation between the sensing and sharing areas.) The active node is defined here as the sensing node that has no on-going transmissions in its sensing area. In this subsection, we derive N_a, the number of active nodes in H when the number of initially deployed sensing nodes in H is given N[3]. The CS results for each sensing node in H is random. Therefore, N_a is a RV that varies within $[0, N]$.

For a sensing node in H to be active, two conditions must be satisfied: the CS result sensed from its sensing area must be idle and that sensed from H must also be idle. We investigate the former event in this section. The resulting N_a becomes the input variable to the DCF behavior analysis in H, which is shown in Section III-B.1.

In summary, since the areas of overlapped regions among sensing areas are varied due to the different locations of the sensing nodes in H and the activities of nodes in those overlapped regions affect multiple corresponding sensing nodes simultaneously, the CS result of a typical sensing node in H cannot be modeled independently. Instead, by splitting a typical sensing area into three equally sized and disjoint

[3]By the homogeneous PPP property, it is not necessary to put any subscript or superscript of H on these variables.

$$B_a^{BAS}(j) = \frac{1}{\mathbb{E}[T_v^{BAS}]} \cdot \begin{cases} \sigma p_a(0) + (sifs + difs)p_a(1) + difs(1 - p_a(0) - p_a(1)), & j = 0 \\ (PHY + \lceil \frac{(MAC+PAY)}{R_s} \rceil T_s + ACK)p_a(1), & j = 1 \\ (PHY + \lceil \frac{(MAC+PAY)}{R_s} \rceil T_s)p_a(j), & 2 \le j \le a. \end{cases} \tag{12}$$

$$B_a^{RTS}(j) = \frac{1}{\mathbb{E}[T_v^{RTS}]} \cdot \begin{cases} \sigma p_a(0) + (3sifs + difs)p_a(1) + difs(1 - p_a(0) - p_a(1)), & j = 0 \\ (RTS + CTS + PHY + \lceil \frac{(MAC+PAY)}{R_s} \rceil T_s + ACK)p_a(1), & j = 1 \\ RTS \cdot p_a(j), & 2 \le j \le a. \end{cases} \tag{13}$$

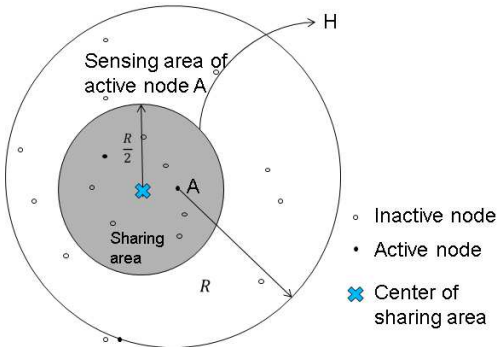

Fig. 3. If we pick up a certain sharing area, every transmitting node in that area has its own sensing area. If there is no on-going transmission in its sensing area, that node is the active node.

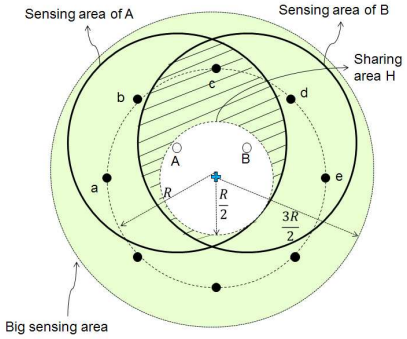

Fig. 4. *Sensing areas* of multiple nodes of a *sharing area*. There are two nodes $\{A, B\}$ in a sharing area. Sensing areas of two nodes include three black dots, $\{a, b, c\}$ and $\{c, d, e\}$ respectively. The hashed region is overlapped by both of sensing areas of node A and B. A dot (c) is included in this overlapped region, and means the quantized space occupied by this region.

subspaces, we can quantize the area of the overlapped region in the unit of $|H|$ where $|\cdot|$ is the cardinality of the set. Then, by accounting for the combinations of the activities of each quantized area and the possible sensing node locations, we can find the distribution of N_a as in (17) with the unknown variable p_{on}. The following section contains the details of the derivations.

1) Details of analysis: The following proposition gives the grounds for splitting a typical sensing area.

Proposition 1. Each sensing area can be thought of as the union of three independent, equally sized and mutually disjoint areas, and the size of this area is the same as $|H|$.

Proof. By the homogeneity of PPP, i.e., the point process is characterized by the area of the space not by the location or shape (See (24) in Appendix), the size of the sensing area is $\frac{3\pi R^2}{4}$, which is three times that of the sharing area. Therefore, if we measure the sensing area and compare it with the size of sharing area, we find that three sharing areas constitute one sensing area. ■

By **Proposition 1**, for one of the sensing nodes in H to be an active node, there should not be any transmission in any of these three independent areas, of which the size is $|H|$. Since, the point deployment is only specified by the size of the space, the probability that a node in H is an active node with only the sensing area considered is again a function of the activity in three subspaces, of which the size is the same as $|H|$. From this, that probability is

$$(1 - p_{on})^3. \tag{14}$$

For example, if there is only one initially deployed node in H, the number of active nodes in that area has a simple PMF given by:

$$\mathbb{P}[N_a = a] = \begin{cases} (1 - p_{on})^3, & a = 1 \\ 1 - (1 - p_{on})^3, & a = 0. \end{cases} \tag{15}$$

However, if multiple nodes are deployed in H, their CS operations are not independent of each sensing node since the sensing area of each node must partially overlap, as in Fig. 4.

Due to this partial dependence of CS among multiple sensing nodes, the probability that a node in H is an active node is not straightforward like (15). The exact dependent CS probability cannot be derived since, to the best of our knowledge, even state-of-the-art research on stochastic geometry cannot reveal the exact distribution on the overlapped area when circles are deployed by PPP [12]. Therefore, we use a spatial quantization approximation, in which some evenly distributed dots are the measure of the overlapped sensing area. To do this, we introduce a large circle with radius $\frac{3R}{2}$ that can cover the sensing areas of all possible nodes in H. We call this circle a *big sensing area*. There are eight dots in the large sensing area. They are evenly distributed in terms of the angle. As depicted in Fig. 5, any sensing node in H includes three dots, except for the case in which the sensing node is located exactly at the center of H.

Proposition 2. When eight dots are evenly distributed on the circumference of a circle of radius R, the sensing area of any sensing node in H covers three consecutive dots.

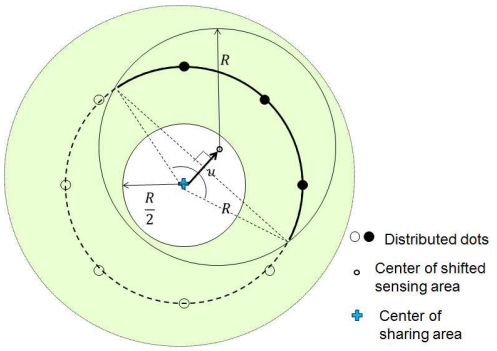

Fig. 5. Each sensing area includes 3 consecutive dots in the *big sensing area*. Each dot represents one of three sensing areas.

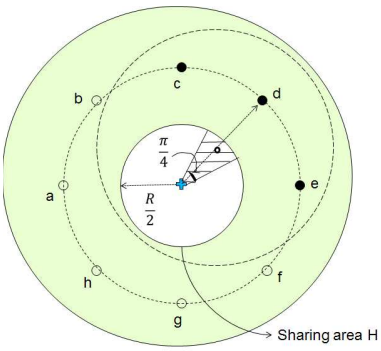

Fig. 6. The hashed region is the possible region of a sensing node having three-consecutive-dots $\{c, d, e\}$. This area has the angle of $\frac{\pi}{4}$ which is split evenly by a direction to the center dot of $\{c, d, e\}$. If $\{c, d, e\}$ are all 'off', this $\{c, d, e\}$ becomes *three-offs*. The number of three-offs is bounded in $[0, 8]$ in H.

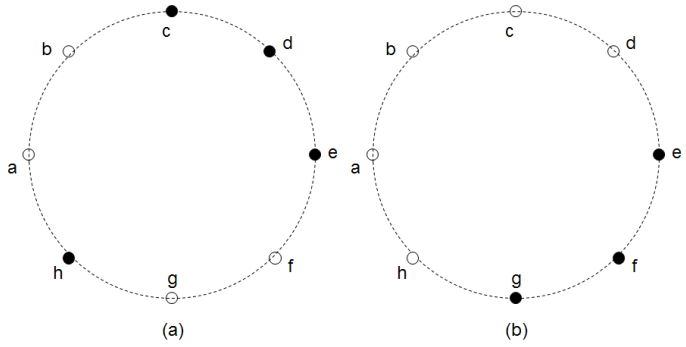

Fig. 7. Example of counting three-offs. If the solid dot means 'off', $\eta = 1$ in both cases, while $D = 4$ and 5 in (a) and (b) respectively. By counting all on-off combinations, we obtain Table I.

TABLE I
O_η^D

	D									
η	0	1	2	3	4	5	6	7	8	Sum(η)
0	0	0	0	8	38	48	28	8	1	131
1	0	0	0	24	24	8	0	0	0	56
2	0	0	12	16	8	0	0	0	0	36
3	0	0	8	8	0	0	0	0	0	16
4	0	0	8	0	0	0	0	0	0	8
5	0	8	0	0	0	0	0	0	0	8
6	0	0	0	0	0	0	0	0	0	0
7	0	0	0	0	0	0	0	0	0	0
8	1	0	0	0	0	0	0	0	0	1
Total	1	8	28	56	60	56	28	8	1	256

Proof. Let vector u characterize the shifting of the sensing area from the center of the large sensing area to a random position. The circumference of the original sensing area partially overlaps the shifted one. This partial circumference (the thick segment of the line in Fig. 5) has an angle measured at the center of the sharing area, which is $2cos^{-1}(\frac{|u|}{R})$. Since $0 < |u| \leq \frac{R}{2}$ by the definition of u, the angle derived from u is bounded in the interval $(\frac{\pi}{3}, \pi]$. This angle always includes three consecutive dots. ■

We measure the overlapped sensing area using these dots. The number of dots included in the intersection of any sensing areas denotes the corresponding overlapped area in the unit of $|H|$. *Each dot represents the boolean indicating whether there is a transmission or not in the corresponding overlapped area in the unit of* $|H|$. Each dot is "on" with p_{on} and "off" with $1 - p_{on}$, where p_{on} for all dots is the same and the on-off boolean are independent of each other. The sensing area of any node in the sharing area can be mapped into one of three-consecutive-dots by **Proposition 2.**

Conversely, the possible region of a sensing node having the same three-consecutive-dots exists in H as in Fig. 6. All sensing nodes located in this region follow the same CS result, i.e., on-off. For example, three consecutive dots of "off" mean that the sensing area having these dots does not have any transmission in its area. The corresponding sensing node is *active*. In contrast to this, if there is at least one of the 'on' dots among the three, this means that the corresponding sensing node is *inactive*.

Any random position of a sensing node in H can be mapped into one of eight three-consecutive-dots and each dot has the probability to be on of p_{on}. Therefore, the problem to find active nodes given N initially deployed nodes in H is solved in two stages. The first stage is to examine the case where three-consecutive-dots are all in "off" states when each dot behaves on-off independently. The second stage is to find how many of these three-consecutive-dots in the "off" state (simply say *'three-offs'*) are picked up through N independent choices. The number of all possible sequences of eight binary digits (representing the on-off states of a dot) are $2^8 = 256$. By counting all combinations of these digits, we derive the PMF of the number of three-offs. Let us denote the number of three-offs by η. For the values of $\eta = \{0, 1, 2, 3, 4, 5, 6, 7, 8\}$, the number of occurrences of each η is $\{131, 56, 36, 16, 8, 8, 0, 0, 1\}$, respectively. These numbers are obtained simply by counting consecutive three-offs in all combinations of eight binary digits (or dots), as shown in Fig. 7.

These occurrences are also categorized according to the number of "on" dots among eight dots, which is denoted by D. By counting each combination, we obtain the quantity O_η^D, the number of occurrences that D out of eight is "on" dots when there are η of three-offs, as in Table I.

Therefore, the probability that there are η three-offs given

p_{on} is:

$$p_\eta = \mathbb{P}[\eta \text{ three-offs}] = \sum_{D=0}^{8} O_\eta^D p_{on}^D (1-p_{on})^{8-D}. \quad (16)$$

Once p_{on} is given, p_η is determined using this equation. Since uniformly deployed sensing nodes in H have any three consecutive dots by **Proposition 2**, becoming an active node is equal to the event that the sensing area of that sensing node has one of η three-offs. Therefore, the probability that a sensing node uniformly deployed in H becomes an active node is $\frac{\eta}{8}$ ($\eta = 0, 1, \ldots, 8$). A sensing node is located in H uniformly and independently. Hence, if there are n sensing nodes in H, the event that a out of n sensing nodes become active nodes is equal to the Bernoulli process with the parameter $\frac{\eta}{8}$. Then, $N_a \sim \mathrm{B}(n, \frac{\eta}{8})$. Let us define $P_{n,a,\eta}$ as the probability that a out of n sensing nodes have one of η three-offs when η is given. Then,

$$P_{n,a,\eta} = \mathbb{P}[N_a = a | n, \eta] = \binom{n}{a} \left(\frac{\eta}{8}\right)^a \left(1 - \frac{\eta}{8}\right)^{n-a}.$$

Finally, N_a is bounded in $[0, N]$ and the conditional probability that $N_a = a$ given $N = n$ is:

$$\mathbb{P}[N_a = a | N = n] = \sum_{\eta=0}^{8} P_{n,a,\eta} p_\eta, \quad a = 0, \ldots, n. \quad (17)$$

D. Effective active node density

We introduced a sharing area; using the spatial boundary of the boolean CS operation and derived the number of nodes distribution therein, which is $\mathbb{P}[N = n]$ as in (5), through the Section III-A. Using the sensing area concept, we derived the number of active nodes in a sharing area, $\mathbb{P}[N_a = a | N = n]$ as in (17) in Section III-C. Based on these derivations, the power distributions in a sharing area, (12) and (13) are derived in Sections III-B.1 and III-B.2. These results are all based on the value of p_{on}, the probability that a sharing area is busy.

The power distributions $B_a(j)$ of (12) and (13) are conditioned on N_a, while N_a is conditioned on N. Therefore, the marginal PMF of p_{on} is obtained by summing all of the probabilities on conditioned variables, as in (18). The condition on N_a is eliminated using (17). The condition on N is eliminated by the homogeneity of PPP, i.e., every geometric subset satisfies Poisson distribution on the number of points in that subset, i.e., (5).

In (18), (a) is from the fact that the possibility of a sharing area being "on" is zero when there is no initial deployed nodes and active nodes. (b) is from (5) and (17). (c) is from (16). In this equation, p_η includes p_{on} term, which is also the marginal PMF from the unconditional event of channel busyness. Therefore, Equation (18) has the unknown variable p_{on} on both sides of the equation and

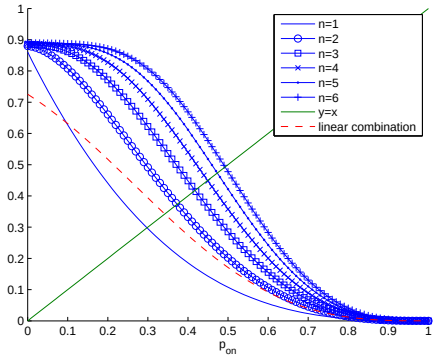

Fig. 8. Each curve represents $\sum_{a=1}^{n} \sum_\eta P_{n,a,\eta} \{\sum_D O_\eta^D p_{on}^D (1-p_{on})^{8-D}\} \sum_{j=1}^{a} B_a(j)$ of Equation (18) when p_{on} is varying and the value of n is given. The right hand side of Equation (18) is the linear combination of these curves. The intersection of this and $y = x$ means the solution p_{on}^*. This figure is for the case of $\lambda = 0.0004$ and other parameters are in Table III.

the solution can be obtained by solving the weighted eighth order polynomial of p_{on}, where the weight is the product form of Poisson and binomial probabilities. More specifically, $\sum_{a=1}^{n} \sum_\eta P_{n,a,\eta} \{\sum_D O_\eta^D p_{on}^D (1-p_{on})^{8-D}\} \sum_{j=1}^{a} B_a(j)$ is the eighth-order polynomial of the unknown p_{on} and all other terms are known, and $\frac{\{\lambda\pi(\frac{R}{2})^2\}^n}{n!} e^{-\lambda\pi(\frac{R}{2})^2}$ is a constant from Poisson distribution for the given n. Therefore, summing the product of these two terms for varying n from $n = 1$ to $n = \infty$ also results in an eighth-order polynomial. Since there is no general solution for polynomials with order higher than four and n goes to infinity, we cannot derive the closed form expression of p_{on}^*, the solution of p_{on}. However, we can still get a solution by finding the intersection of the right hand side and left hand side of (18). For computational simplicity, we use six instead of infinity for the value of n, as shown in Fig. 8. The rate of increase of the curves due to increasing n diminishes and the coefficient from Poisson distribution also rapidly decreases over higher n. Therefore the curve of $n = 6$ is sufficiently close to the asymptotic curve. (We verify that this simplification is sufficient to reflect the original equation by comparing our analysis and simulation results in the next section.)

If we obtain p_{on}^*, the distribution of the number of transmitting nodes in a sharing area can be derived as in (21), where the number of transmitting nodes in a sharing area is denoted by Z. The expected number of transmitting nodes is derived from this result.

$$\mathbb{E}[Z] = \sum_{z=0}^{\infty} z \cdot \mathbb{P}[Z = z] \quad (19)$$

The effective active node density is defined as the average number of transmitting nodes per unit area. Thus, we finally obtain the effective active node density as follows:

$$\lambda' = \frac{\mathbb{E}[Z]}{\pi(\frac{R}{2})^2}. \quad (20)$$

This is used in the cumulative distribution function (CDF) (31) and the probability density function (PDF) (32) of the

$$
\begin{aligned}
p_{on} &= \sum_{n,a}\sum_{j=1}^{a} B_a(j) = \sum_{n=0}^{\infty}\mathbb{P}[N=n]\sum_{a=0}^{n}\mathbb{P}[N_a=a|N=n]\sum_{j=1}^{a}B_a(j) \overset{(a)}{=} \sum_{n=1}^{\infty}\mathbb{P}[N=n]\sum_{a=1}^{n}\mathbb{P}[N_a=a|N=n]\sum_{j=1}^{a}B_a(j) \\
&\overset{(b)}{=} \sum_{n=1}^{\infty}\frac{\{\lambda\pi(\frac{R}{2})^2\}^n}{n!}e^{-\lambda\pi(\frac{R}{2})^2}\sum_{a=1}^{n}\sum_{\eta}P_{n,a,\eta}p_{\eta}\sum_{j=1}^{a}B_a(j) \\
&\overset{(c)}{=} \sum_{n=1}^{\infty}\frac{\{\lambda\pi(\frac{R}{2})^2\}^n}{n!}e^{-\lambda\pi(\frac{R}{2})^2}\sum_{a=1}^{n}\sum_{\eta}P_{n,a,\eta}\{\sum_{D}O_{\eta}^{D}p_{on}^{D}(1-p_{on})^{8-D}\}\sum_{j=1}^{a}B_a(j) \qquad (18)
\end{aligned}
$$

TABLE II
SIMULATION PARAMETERS FOR MHC AND SSI PROCESSES.

Fixed Parameters	
Transmission power (p)	0.001(W)
Background Plane	Circle ($B(O,R)$)
Radius of Background Plane ($R_M = R_S$)	282 (m)
Exclusion Ball Radius (r)	70 (m)
Number of Iterations (n)	100000
Channel Model	$\frac{X}{d^4}$, where $X \sim \text{Exp}(1/p)$
Varying Parameters	
Node Density (λ)	$\{1,2,3,4,5\} * 10^{-4}$

aggregate interference in the Appendix. We plot the resulting PDF for varying network parameters and compare this with the simulation results in Section IV.

IV. VERIFICATION OF THE ANALYSIS

In this section, we first, plot the analyzed p_{on} and λ', and plot the PDF (32) and CDF (31) of the aggregate interference using this λ'. Next, we compare these derived results with the results of NS-2 simulations and two other dependent point process simulations. For all simulation scenarios, the exclusion radius r in dependent processes are given to 70 (m). In the NS-2 simulation, MAC/PHY parameters and channel model are given so that the CS radius R is determined to be between 50 and 100 (m) for investigation of p_{on} and λ'. We later change these parameters for R to be equal to 70 (m) for the comparison with the dependent point process.

A. Simulation setup

1) Monte Carlo simulation for MHC and SSI: We deployed the points using MHC and SSI processes, explained in [5], with Matlab. The parameters used in the simulations are listed in Table II[4]. For a given number of nodes, the aggregated power was measured at O the center of ball B with radius R_M or R_S for MHC or SSI respectively. The number of deployed nodes was generated using CDF of Poisson distribution with the parameter $\lambda|B|$ where λ is the initial node density and $|B|$ is the area of ball B. We deployed these points uniformly and measured the aggregate power at O. We repeated this procedure for more than 100,000 iterations.

[4]Refer to the paper [5] for the meaning of parameters and details of the process.

2) NS-2 simulation for PPP: To verify the analysis results, we conducted simulations using NS-2 [13]. Unlike the previous version, NS-2 version 2.34 (released June 2009), includes wireless PHY and MAC layer patches for the realistic IEEE 802.11 DCF standard [14]. This enabled us to realistically simulate the PHY and MAC stack of IEEE 802.11 DCF. The simulation parameters, which are the default ones for IEEE 802.11a PHY and MAC, are listed in Table III. They are from the previous research [15].

The overall simulation procedure consisted of genuine NS-2 simulations, pre-processing of the scenario, and post-processing of the data, as shown in Fig. 9. Generating the number of transmitting nodes using Poisson distribution, deploying them uniformly, attaching designated receiving nodes to each transmitting node, and generating traffic for each transmitting node were done in the pre-processing stage. For the saturated traffic situation, we obtained the time duration from $\max_i\{$the first transmission of node $i\}$ to $\min_i\{$the last transmission of node $i\}$. We call this the time window. Finding the time window, measuring the received power at the measuring node, recording the lasting time of each received power value, and accumulating all the measurements were done in the post-processing stage.

In attaching the receivers to transmitters, we fixed the relative location of each receiver at 5 (m) right and 5 (m) up from its transmitter. To measure the aggregate power, we put the measuring node in the center of the simulation grid. This node then reported on the received power level and we recorded the lasting time and power level of each received signal.

The simulation conducted in this paper is large-scaled; the reasons are two. First, each simulation per geometry scenario takes a long time. This time includes the simulation time in NS-2 and the post-processing time for handling received power instances. NS-2 traces all of the packet-level transactions with the received power recorded at every receiver. In post-processing stage, calculation of the received power from all of the on-going transmissions at a measuring node takes computation time. Moreover, the simulation time itself (not the computation time) has to be long enough to reflect the steady-state behavior, which theoretically requires infinite investigation time. We consider at least 30 seconds per scenario as the simulation time (this takes about 2 h in real time using a Quad core i7 processor computer). Second, to get the sound statistical inference of PPP, we repeat per-geometry simulation many times. We do 50 repetitions, since all the resulting PDFs of aggregate interference obtained from the simulations show

$$\mathbb{P}[Z=z]=\sum_{n=z}^{\infty}\frac{\{\lambda\pi(\frac{R}{2})^2\}^n}{n!}e^{-\lambda\pi(\frac{R}{2})^2}\cdot\sum_{a=z}^{n}\sum_{\eta}P_{n,a,\eta}\{\sum_{D}O_{\eta}^{D}(p_{on}^{*})^{D}(1-p_{on}^{*})^{8-D}\}B_a(z),\ \text{for } z\in\{0,1,\dots\} \tag{21}$$

TABLE III
SIMULATION PARAMETERS FOR NS-2.

Fixed Parameters	
Background Grid	Regular Rectangular
Grid Size	500(m)*500(m)
Transmission power	0.001(W)
Initial window size W_0	16
Maximum backoff stage m	6
CW min/max	15/1023
Slot Time (σ)	9(us)
SIFS	16(us)
DIFS	sifs+2σ=34 (us)
Short Retry Limit K	7
Long Retry Limit K	4
PLCP Preamble Duration	16 (us)
PLCP Header duration except Service field	20(us)
OFDM Symbol Duration	4(us)
IFQ Length	50
RTS MPDU + Service + Tail Field	182(bits)
CTS MPDU + Service + Tail Field	134(bits)
ACK MPDU + Service + Tail Field	134(bits)
Data Rate	6(Mbps)
Control Rate	1(Mbps)
Modulation	BPSK
Code Rate	1/2
Carrier Frequency	5.18 (GHz)
Preamble Capture Threshold	2.5118
Data Capture Threshold	100
Noise Floor	10^{-12} (W)
Data Type	CBR
CBR Rate	$5*10^6$ (packets per sec)
Number of Packets in the application queue	3000
Varying Parameters	
Payload Size	500 or 1000 (Bytes)
RTS Threshold	0 or 10000
Node Density (λ)	$\{1,2,3,4,5\}*10^{-4}$
Effective CS Range (R)	50, 70, 100(m)

the convergence before 30 repetitions. The simulation time for all 50 scenarios takes approximately four days on average. We repeat this process for each combination of PHY and MAC layer parameters.

The saturated traffic was assigned to all transmitters so that there was no idle time by the traffic itself during the simulations. The background grid for all the simulation scenarios was always same: a square 500 (m) by 500 (m) in size. The transmission times for RTS, CTS, PPDU (PHY+MAC+PAY) with 500 B (or 1000 B) of payload and ACK were 52, 44, 728 (or 1396), and 44 (μs), respectively (see Table III and [15]). We ignored the propagation delay, even though this exists in the simulator, since the value was quite small compared to the other transmission times. A generated traffic of 5,000,000 packets per second (pps) was given to all the transmitters. This means a value of 0.2 (μs) for inter-arrival time from the application layer to the physical layer, which is less than the whole transmission time for one successful packet, i.e., $RTS+CTS+PHY+MAC+PAY+ACK+3*sifs+difs=948(\mu s)$, which is enough for the traffic to be saturated.

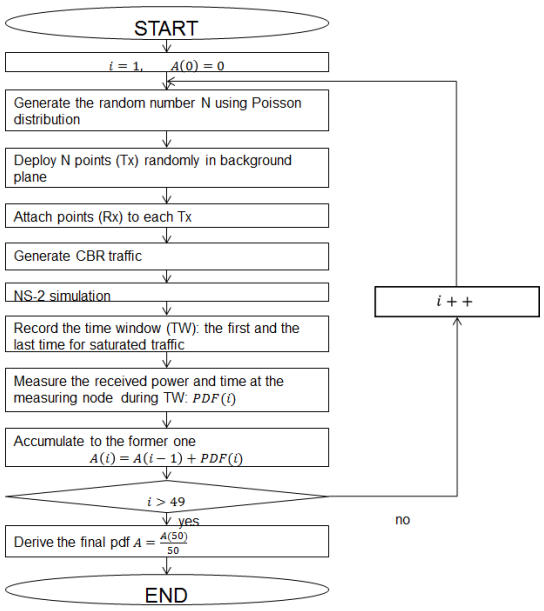

Fig. 9. Simulation flow. For a given combination of λ, PHY and MAC parameter, this procedure is carried out.

B. Discussions

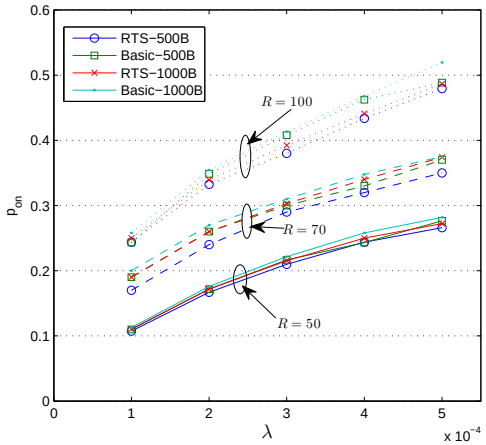

Fig. 10. P_{on} versus λ for all combinations of MAC layer parameters.

1) Analysis results on p_{on} and λ': All p_{on} in this subsection refer to p_{on}^{*}, the final solution of p_{on} for simplicity of expression. In Fig. 10, p_{on} are shown for various combinations of MAC parameters. The factor that affects p_{on} the most is the effective CS distance R, followed by λ, the initial node density. As λ increases, p_{on} naturally increases due to the increased congestion level with semi-log style trend.

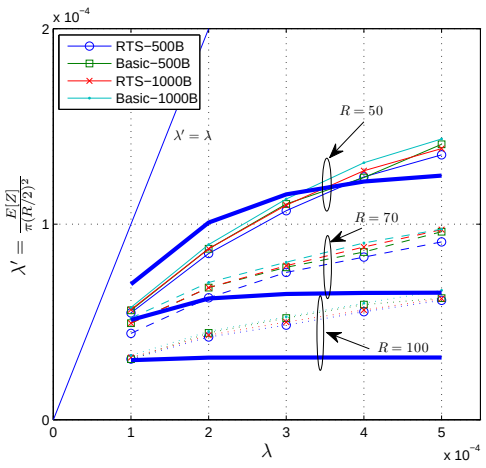

Fig. 11. New node density λ' for initial node density λ and MAC layer parameter combinations. The thicker curves are using λ'' in (22).

If there is only reduced idle time factor without increasing collision probability, as in [8]'s ideal CSMA, the rate of increase of p_{on} must be a log function style. However, our model reflects the increased collision probability and reduced idle time simultaneously, as obtained in real situations. The resulting p_{on} shows a mixture of linear and log functions. Within the same R, the combination of mode and payload size that has the lowest p_{on} is the RTS mode and short payload. In other words, the order of $\{RTS-500B, Basic-500B, RTS-1000B, Basic-1000B\}$ is for lower p_{on}. In general, RTS-CTS mode had a lower congestion level than the basic mode since the system cost was only the RTS-CTS packet collision and waiting time for retransmission compared to basic mode. A large payload in basic mode makes for a higher congestion level. However, in the cases of some λ values, RTS-CTS packets were small enough to compensate for the payload size. Therefore Basic-500B might have higher p_{on} than RTS-1000B. In this case, the effect of mode was weaker than that of the payload size.

This p_{on} was used in the new density λ' (20) and we plotted this as shown in Fig. 11. This figure shows that the smaller R makes for a higher λ', which is the opposite case to p_{on}. This is understandable since a smaller R signifies more insensitivity to the interference around. Therefore, we expected the result of $R = 0$, the ALOHA system, to approach the line $\lambda' = \lambda$ in the figure. This line also represents wireless access systems that have no MAC, such as macro or femto cellular systems. The curve λ' is a version of λ filtered by the CSMA/CA and BEB mechanism. By showing the $\lambda' = \lambda$ line and the curves together, Fig. 11 also addresses how large the gap between these two node densities is and how effectively CSMA/CA MAC operates. The bold curves are from:

$$\lambda'' = \frac{1 - \exp(-\lambda\pi D^2)}{\pi D^2} \tag{22}$$

where D is the exclusion distance with an ambiguity. However, we put R into D in this figure. This expression is the approximated node density for modeling MHC adopted in [3] and [16]. As can be seen in the figure, the variation of λ' is higher than λ'' for varying λ. Since λ'' is used for modeling dependent point processes, it cannot trace the real operation. As shown in the next section, our aggregate power distribution adopting this λ' is the most elaborate among other point processes. Therefore, Fig. 11 shows the gap in aggregate interference between simplified MHC and the real situation. This is significant because this simplified MHC expression is widely used in academia [3], [16], [17].

Finally, our new effective node density and the framework for deriving this can be applied to any other type of aggregate interference problem. In other words, whatever the appearance of the PDF, λ, the original node density can be substituted for λ', the new effective node density, using our derivation framework.

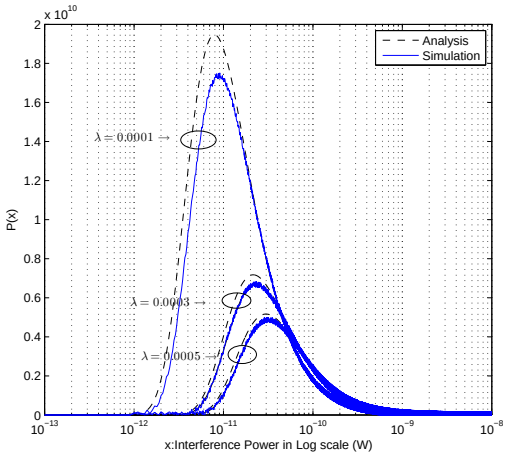

Fig. 12. Probability density of aggregate interference in the condition of RTS mode, 500B payload and $R = 70$(m). Other parameters are in Table III.

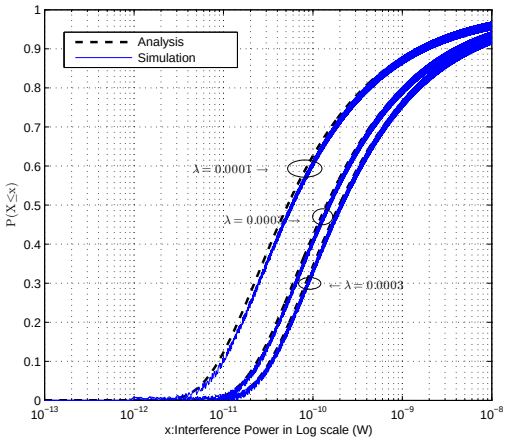

Fig. 13. Cumulative distribution of aggregate interference in the condition of RTS mode, 500B payload and $R = 70$(m).

2) Comparison of the resulting aggregate interference with the simulation: Using this λ' and shot noise analysis, we plotted the distribution of aggregate interference. The PDF and CDF of the analysis in each node density showed high correlations with those of the NS-2 simulations, as seen in Fig.

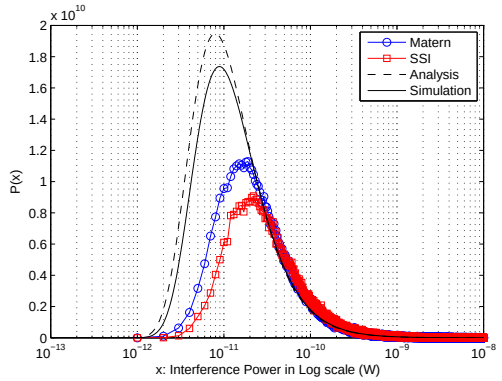

Fig. 14. Probability density of aggregate interference when λ is 0.0001.

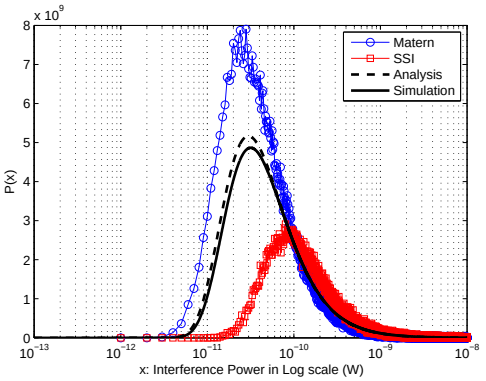

Fig. 16. Probability density of aggregate interference when λ is 0.0005.

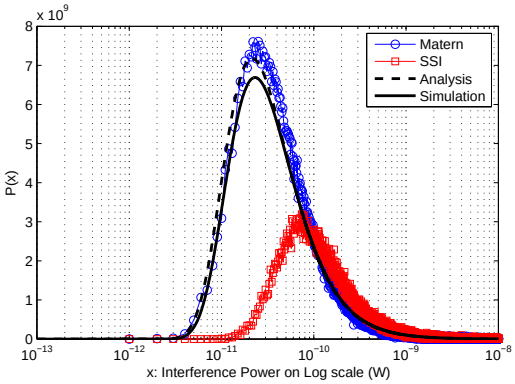

Fig. 15. Probability density of aggregate interference when λ is 0.0003.

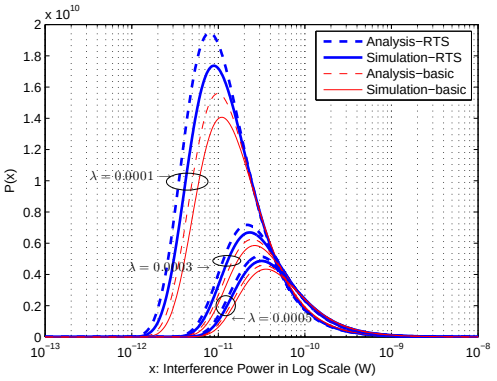

Fig. 17. Probability density of aggregate interference in the case of 500B payload and $R = 70$.

12 and 13. We depict all the PDFs in a log scale. Although at first glance they resemble a log-normal distribution, they are asymmetric based on the main lobe. They show heavy tail properties even in a log scale axis by investigating the following equations:
Normal scale:

$$\lim_{t\to\infty} e^{at}\Pr[I > t] = \lim_{t\to\infty} e^{at}\left(1 - \text{erfc}\left(\frac{\lambda'\pi^2\sqrt{p}}{4\sqrt{t}}\right)\right) = \infty,$$

Log scale:

$$\lim_{t\to\infty} e^{at}\Pr[I > \log t] = \lim_{t\to\infty} e^{at}\left(1 - \text{erfc}\left(\frac{\lambda'\pi^2\sqrt{p}}{4\sqrt{\log t}}\right)\right) = \infty,$$

where I is RV of aggregate interference.

Therefore, they are definitely neither normal nor log-normal distributions. This is notable as some research efforts in the signal processing field assume that the aggregate interference follows normal (in dBm unit) or log-normal (in W unit) distributions. For the other features, the higher the mean of the aggregate power, the lower the probability of that mean value. Therefore, low-mean high-probability and high-mean low-probability patterns are shown in all the results. This is because the total sum of the probability is fixed to 1 and the x-axis is log-scaled and not linear.

Compared with dependent point processes, at any given λ value, our analysis is the closest one to the simulation results, as depicted in Fig. 14-Fig. 16. The interference of MHC is always less than that of SSI since MHC is the lower bound of SSI, which is commented on in [5]. However, these two are not as sensitive as our model to variations in node density. Moreover, these two do not have sufficient MAC and PHY layer parameters to reflect the real situation, while our analysis can model any combination of the system parameters, as in Fig. 17. As shown in the figures so far, our model of interference has slightly lower values than that of the simulation in each case. This is mainly because the simulator allows the *capture* situation. In our analysis, the collision between transmitters is regarded as a failure of transmission and this increases each collided nodes' backoff stages. In contrast, there might be a successful transmission even when multiple nodes in a CS area are transmitting at the same time. This is because if the ratio of one incoming signal to the others is guaranteed to be higher than a certain threshold, this stronger incoming signal can always be decoded[5]. In our analysis, we ignored that situation in order to simplify the analysis. Nevertheless, our result is competitive.

From these results, we learned the following lessons: If the network is required to maintain a lower interference than a certain level, there are multiple combinations of parameters that need to be controlled. Since the PDF of the aggregate interference is a function of λ', there are multiple combinations of parameters that can result in the same value of λ'. Those

[5]The patch in NS-2 has two capture thresholds which are the preamble capture and the data capture. Thus, these two capture events can also occur in the simulations.

controllable parameters are R, transmission mode, payload size, etc. This can be used for the interference management in uncontrolled interference limited systems such as cognitive radio networks. In addition, this statistical information helps to quantify the spectrum opportunity in cognitive radio networks such as exploited in [18]. In addition, the interaction among heterogeneous systems using the same frequency band such as in WLANs, ZigBee, and Bluetooth can be understood using this analysis from the perspective of the mutual interference. This knowledge can also be used to measure the energy level in the air when wireless power transfer (WPT) systems have some conditional activation mechanisms.

V. Conclusion

In this paper, we analyzed the aggregate interference from randomly deployed CSMA/CA nodes. CSMA/CA MAC operation on the stochastic geometry makes the understanding of a node's behavior difficult. However, the homogeneity of PPP provides a clue to solving the problem. We derived the effective active node density by spatially quantizing the infinite space and analyzing the steady-state power distribution on this quantization unit. Verification is also nontrivial since repetition is needed in order to get sound statistical inference from random topology. Although the elaborate closed form expression of the interference distribution cannot be obtained, the analysis framework proposed in this paper shows high applicability to many related problems in modern wireless networks where the amount of interference in a random node geometry significantly affects system performance.

Appendix

This section can be replaced with reference [6] as long as the readability does not deteriorate.

A. Aggregate power from Nodes under the PPP Geometry

We consider the infinite planar where the transmitting nodes are deployed randomly at positions specified by a Poisson distribution. For the general dimension space $\mathbb{R}^d$ and the locally finite non-null measure Λ, the PPP can be defined:

Definition 2. The PPP Φ of intensity measure Λ is defined by means of its finite-dimensional distributions

$$\mathbf{P}\{\Phi(A_1)=n_1,\ldots,\Phi(A_k)=n_k\}=\prod_{i=1}^{k}\left(e^{-\Lambda(A_i)}\frac{\Lambda(A_i)^{n_i}}{n_i!}\right), \tag{23}$$

for every $k=1,2,\ldots$ and all bounded, mutually disjoint sets A_i for $i=1,\ldots,k$. If $\Lambda(dx)=\lambda dx$ is a multiple of Lebesgue measure (volume) in $\mathbb{R}^d$, we call Φ a homogenous PPP and λ is its intensity parameter.

Simply, in 2D homogeneous PPP, the probability that the area S has k nodes is:

$$P(k)=e^{-\lambda S}\frac{(\lambda S)^k}{k!}, \tag{24}$$

where λ is constant for all disjointed and bounded area S.

Proposition 3.(Proposition 1.2.2 in [6]) The Laplace functional of PPP of intensity measure Λ is

$$\mathcal{L}_\Phi(f)=e^{-\int_{\mathbb{R}^d}(1-e^{-f(x)})\Lambda(dx)}, \tag{25}$$

where d is the dimension of point deployment and f is the probability function of the point position. See the [6] for the proof.

A shot-noise field is non-negative vector random field $I_{\tilde{\Phi}}(y)$ defined for all y in some Euclidean space and which is a functional of a marked point process $\tilde{\Phi}$. Here is a list of arguments dimensions related to this field: All $y\in\mathbb{R}^{d'}$; $I_\Phi(y)\in\mathbb{R}^{+k}$ for all y; and this is generated by a marked point process $\tilde{\Phi}=\sum_i \varepsilon_{(x_i,m_i)}$ on $\mathbb{R}^d$ with marks in $\mathbb{R}^l$ where ε is a Dirac measure; and non-negative response function $L=(L_1,\ldots,L_k)$. Therefore the total dimension input and output arguments of shot noise field is $\mathbb{R}^{d'}\times\mathbb{R}^d\times\mathbb{R}^l\to(\mathbb{R}^+)^k$.

Definition 3. The shot noise field associated with the marked point process $\tilde{\Phi}$ and the response function $L=(L_1,L_2,\ldots,L_k)$ is

$$I_{\tilde{\Phi}}(y)=(I_1(y),\ldots,I_k(y))=\sum_{(x_i,m_i)\in\tilde{\Phi}}L(y,x_i,m_i), \tag{26}$$

where the sum is evaluated component-wise for the vector response model L.

Proposition 4.(Proposition 2.2.4 in [6]) Suppose that $\tilde{\Phi}$ is an independent marked PPP with intensity measure Λ and mark distribution $F_x(\mathrm{d}m)$. Consider the Shot Noise $I(y)=I_{\tilde{\Phi}}(y)$ with response function L. Then

$$\mathcal{L}_{I(y)}(s_1,s_2,\ldots,s_k)$$
$$=\exp\left\{-\int_{\mathbb{R}^d}\int_{\mathbb{R}^\ell}\left(1-e^{-\sum_{i=1}^k s_i L_i(y,x,m)}\right)F_x(\mathrm{d}m)\Lambda(\mathrm{d}m)\right\}. \tag{27}$$

See the [6] for proof.

Here $L_i(y,x,m)$, the element of the response function L represents the i-th channel link gain function out of k ones with the measuring location y, transmitter position x and mark m. The total power received from this collection of transmitters at a given measuring location is in essence a shot-noise field. Applying this proposition to our CSMA/CA random network in an infinite planar with omni-directional antennas, the shot noise model consists of 4 components. 1) at a measuring location in 2-D planar ($d'=2$); 2) collection of points representing the locations of transmitters on the plane $\mathbb{R}^2$ ($d=2$); 3) marks $m_i=p_i$ representing the powers of the transmitters ($\ell=1$); and 4) a scalar ($k=1$) response function $L(y,x_i,p_i)=p_i/l(|x_i-y|)$, where $l(r)$ is the omni-directional path-loss function of distance r. According to whether the points deployment and the assignment of mark to a point are deterministic or stochastic, the standard stochastic scenario is categorized. Our model is M/M[6], one of the four scenarios, which means the mixture of Poisson point process and exponential RV assignment for a mark assignment.

[6]M/M is the expression of Kendall like notation which means Markov point deployment and Markov mark assignment in the standard stochastic scenario.

For the general $l(r)$ and $G(s) = \Pr[p_i < s]$, Proposition 4 leads

$$\mathcal{L}_{I(y)}(s) = \mathcal{L}_I(s) = \exp\left\{-2\pi\lambda \int_0^\infty r(1 - \mathcal{L}_p(s/l(r)))\mathrm{d}r\right\}, \quad (28)$$

where $\mathcal{L}_p(t) = \int_0^\infty e^{-ts} G(\mathrm{d}s)$ is the Laplace transform of the transmitted power.

We use the simplified pathloss function, $l(r) = (Ar)^\beta$ where $A > 0$, $\beta > 2$ for an omni-directional antenna case. For the power reception model, we use the *virtual power model* where each transmitting node assumes to emit a random power not the deterministic one and there is only pathloss effect in the channel link gain. In other words, p_i, the transmission power at node i equals $P_i F$ where P_i is the constant value and F is independent and identically distributed RV. And the received power at the measuring location originated from the node i is $l(r_i)p_i$ where r_i is the distance between node i and the measuring location. For modeling Rayleigh fading channel, we assume that F is exponential RV with unit mean. And P_i is constant p for all transmitting nodes i. Then, p_i is exponential RV with the mean $p \cdot 1$, i.e., $p_i \sim \mathrm{Exp}(\frac{1}{p})$ and $G(s) = \Pr[p_i < s] = 1 - e^{-\frac{s}{p}}$ and we get following equations, which are Eq. (2.25) and (2.26) in [6]:

$$\mathcal{L}_I(s) = \exp\left\{-\lambda\,(ps)^{2/\beta}\,\frac{K(\beta)}{A^2}\right\}, \quad (29)$$

where $K(\beta) = \frac{2\pi^2}{\beta \sin(2\pi/\beta)} = \frac{2\pi\Gamma(2/\beta)\Gamma(1-2/\beta)}{\beta}$.

Unfortunately, there is no known closed form of I for general β but 4 since the inverse Laplace transform does not exist for all β cases. From now on, we only consider $A = 1$ and $\beta = 4$ case. Let f and F denote PDF and CDF of the same RV respectively, then $f(t) = \frac{dF(t)}{dt}$ holds. From $\mathcal{L}_f(s) = s \cdot \mathcal{L}_F(s)$, we have the Laplace transform of CDF of RV I,

$$\mathcal{L}_{F_I}(s) = \frac{\exp\{-\lambda K(4)\sqrt{ps}\}}{s}. \quad (30)$$

Using the fact that inverse Laplace transform of $\frac{\exp(-a\sqrt{s})}{s}$ is $\mathrm{erfc}(\frac{a}{2\sqrt{t}})$ when $a \geq 0$, we obtain CDF and PDF of RV I similarly in [10]:

$$F_I(t) = \mathrm{erfc}\left(\frac{\lambda\pi^2\sqrt{p}}{4\sqrt{t}}\right), \quad (31)$$

$$f_I(t) = \frac{\exp(\frac{-\pi^4\lambda^2 p}{16t})\pi^{3/2}\frac{\lambda}{p}}{4(\frac{t}{p})^{3/2}}, \quad (32)$$

where $\mathrm{erfc}(x) = \frac{2}{\sqrt{\pi}}\int_x^\infty e^{-t^2}\mathrm{d}t$ is a complementary error function.

REFERENCES

[1] M. K. Karakayali, G. J. Foschini, and R. A. Valenzuela, "Network coordination for spectrally efficient communications in cellular systems," *IEEE Wireless Commnications*, Vol. 13, No. 4, pp. 56-61, Aug., 2006.

[2] D. Lopez-Perez, I. Guvenc, G. D. L. Roche, M. Kountouris, T. Q. S. Quek, and J. Zhang, "Enhanced intercell interference coordination challenges in heterogeneous networks," *IEEE Wireless Communications*, Vol. 18, No. 3, pp. 22-30, Jun., 2011.

[3] F. baccelli, B. Blaszczyszyn, and P. Muhlethaler, "An Aloha protocol for multihop mobile wireless networks, " *IEEE Trans. on Information Theory*, Vol. 52, No. 2, pp. 421-436, 2006.

[4] J. Andrews, R. K. Ganti, M. Haenggi, N. Jindal, and S. Weber, "A primer on spatial modeling and analysis in wireless networks," *IEEE comm. magazine*, Vol. 48, No. 11, pp. 156-163, 2010.

[5] A. Busson, G. Chelius, and J.-M. Gorce, "Interference Modeling in CSMA Multi-Hop Wireless Networks," *Technical report INRIA*, inria-00316029-ver3, pp. 1-21, 2009.

[6] F. baccelli, and B. Błaszczyszyn, "Stochastic Geometry and Wireless Networks Volume 1: THEORY," *Foundations and Trends in Networking*, Vol. 3, No. 3-4, pp. 249-449. 2009.

[7] J. Rice, "On generalized shot noise," *Advances in applied probability*, Vol. 9, No. 3, pp. 553-565, 1977.

[8] L. Jiang, and J. Walrand, "A distributed CSMA algorithm for throughput and utility maximization in wireless networks," *IEEE/ACM Trans. on Networking*, Vol. 18, No. 3, pp. 960-972, 2010.

[9] G. Bianchi, "Performance Analysis of the IEEE 802.11 Distributed Coordination Function," *IEEE Journal of Sel. Areas on Comm.*, Vol. 18, No. 3, pp. 535-547. 2000.

[10] J. Hwang, and S.-L. Kim, "Cross-Layer Optimization and Network Coding in CSMA/CA-Based Wireless Multihop Networks," *IEEE/ACM Trans. on Networking*, Vol. 19, No. 4, pp. 1028-1042, 2011.

[11] Standard "Performance Analysis of the IEEE 802.11 Distributed Coordination Function," *IEEE STA*, Vol. 18, No. 3, pp. 535-547. 2007.

[12] R. Herczynski, "Distribution function for random distribution of sh-peres," *Nature*, Vol. 255, pp. 540-541, 1975

[13] Network Simulator-2 http://isi.edu/nsnam/ns/

[14] Q. Chen, F. Schmidt-Eisenlohr, D. Jiang, M. Torrent-Moreno, L. Del-grossi, and H. Hartenstein, "Overhaul of IEEE 802.11 Modeling and Simulation in NS-2," *Proc. ACM MsWiM 07*, 2007

[15] D. Qiao, S. Choi, and K. G. Shin, "Goodput Analysis and Link Adaptation for IEEE 802.11a Wireless LANs," *IEEE Trans. on Mobile Computing*, Vol. 1, No. 4, pp. 278-292, 2002.

[16] D. Stoyan, W. S. Kendall, and J. Mecke, "Stochastic geometry and its applications," *John Wiley and Sons*, pp. 1-345, 1987.

[17] M. Haenggi, and R. K. Ganti, "Interference in Large Wireless Net-works," *Foundations and Trends in Networking*, Vol. 3, No. 2, pp. 127-248 2009.

[18] J. Hwang, and C.-B. Chae, "Optimal operation boundary based on network density for super WiFi systems," In preprint.